Journal of Biomedical Optics

SPIEDigitalLibrary.org/jbo

Orientational dynamics of human red blood cells in an optical trap

Praveen Parthasarathi
Belavadi V. Nagesh
Yogesha Lakkegowda
Shruthi S. Iyengar
Sharath Ananthamurthy
Sarbari Bhattacharya

SPIE

Orientational dynamics of human red blood cells in an optical trap

Praveen Parthasarathi, Belavadi V. Nagesh, Yogesha Lakkegowda, Shruthi S. Iyengar, Sharath Ananthamurthy, and Sarbari Bhattacharya
Bangalore University, Department of Physics, Bangalore, 560056, India

Abstract. We report here on studies of reorientation of human red blood cells (RBCs) in an optical trap. We have measured the time required, t_{re}, for the plane of the RBC entering the optical trap to undergo a 90-deg rotation to acquire an edge on orientation with respect to the beam direction. This has been studied as a function of laser power, P, at the trap center. The variation of t_{re} with increasing P shows an initial sharp decrease followed by a much smaller rate of further decrease. We find that this experimentally measured variation is not in complete agreement with the variation predicted by a theoretical model where the RBC is treated as a perfectly rigid circular disk-like body. We argue that this deviation arises due to deformation of the RBC. We further reason that this feature is dominated by the elastic behavior of the RBC membrane. We compare the studies carried out on normal RBCs with RBCs where varying conditions of membrane stiffness are expected. We propose that the value of energy used for maximum deformation possible during a reorientation process is an indicator of the membrane elasticity of the system under study. [DOI: 10.1117/1.JBO.18.2.025001]

Keywords: red blood cell; optical tweezers; cell membrane elasticity.

Paper 12556 received Aug. 27, 2012; revised manuscript received Dec. 13, 2012; accepted for publication Jan. 3, 2013; published online Feb. 4, 2013.

1 Introduction

An asymmetric microstructure in a laser tweezer orients itself such that maximum of its volume lies in the region of highest electric field.[1–3] Thus equilibrium orientations of asymmetric microstructures in an optical trap are strongly dependent on the shapes of the microstructure as well as the laser beam. Yet another aspect deciding the orientation of microstructures in an optical tweezer is birefringence. It is seen that microstructures with negative birefringence align with their slow axis along the plane of vibration in a linearly polarized trap and act as microrotors when subjected to a circularly polarized trap.[4]

A healthy erythrocyte has a biconcave disk-like shape. Upon trapping in a laser tweezer, it acquires an edge-on orientation with respect to the beam direction. Sometimes the erythrocyte has a nonsymmetrical surface morphology, which could be brought about either by disease or by the tonicity of the surrounding medium. In such cases, the edge on orientation is followed by rotation about an axis coincident with the beam direction.[5] This happens irrespective of the polarization of the laser. Rotations can also be brought about in an optical trap, which has an asymmetric distribution of intensity normal to the propagation direction (asymmetric trap).[6] The angular speed of this rotation following the orientation has been found to be dependent on the red blood cells (RBC) membrane stiffness besides the power of the incident beam.[5,6]

It is thereby possible that t_{re}, the time required by the plane of the RBC entering the optical trap to undergo a rotation of 90 deg, thus acquiring an edge on orientation to the beam propagation direction, is also dependent on the RBC membrane stiffness besides the laser power. To explore this further, apart from the measurements carried out on RBCs sourced from healthy individuals with no known medical conditions (*normal* RBC), we have studied RBCs sourced from individuals with established conditions of hyperglycemia (*h*RBC) and those restored consequent to a process of crenation (*r*RBC). Crenation is the contraction of a cell into a scalloped structure due to exosmosis of water on exposure to a solution that is either hypertonic or of pH altered towards acidic conditions. In earlier studies, we have observed higher angular speeds following reorientation for *h*RBCs as compared to *normal* RBCs in asymmetric traps.[6] The higher angular speeds of the *h*RBCs were attributed to increased membrane stiffness and the consequent lowering of overall viscous drag experienced by the cell. We conjecture that RBCs restored from the process of crenation have membrane stiffness lower than that of *normal* RBCs. We garner support for this from the fact that *r*RBCs, in general, have higher values of t_{re} compared to *normal* RBCs at similar laser powers.

2 Experimental Details

2.1 *Sample Preparation*

2.1.1 *Normal RBC*

About 20 μl of freshly drawn blood from a healthy individual was taken in a standard ethylene diamine tetraacetic acid tube and diluted to 2 ml with phosphate buffer saline (PBS) of pH = 7.4, the solutions of PBS having been prepared at various points of time. The RBCs from these suspensions were observed to be free from deformations and identical under a microscope after a nominal passage of time. Measurements were carried out for the RBCs from each of these suspensions

Address all correspondence to: Sarbari Bhattacharya, Bangalore University, Department of Physics, Bangalore, 560056, India. Tel: +91 80 22961479; Fax: +91 80 23219295; E-mail: sarbari.bhattacharya@bub.ernet.in

0091-3286/2013/$25.00

and the results pertaining to each suspension were tabulated and analyzed separately.

2.1.2 *h*RBCs

Blood samples from a volunteer with a well established case of hyperglycemia were obtained. At the time of sample collection, the blood sugar level of the volunteer was recorded to be 290 mg/dl (fasting blood sugar reading) and 340 mg/dl (random blood sugar reading). These were then subjected to the standard procedure of storage as described for *normal* RBCs. The RBCs appeared normal in shape and no asymmetries in surface morphology were seen.

2.1.3 *r*RBCs

Normal RBCs were suspended in PBS of pH 6.3 for about five minutes. This was enough to induce the process of crenation in the RBCs in the sample. At the end of this period, the pH was readjusted to 7.4 by adding 5 μl of 0.1N NaOH solution to the sample. About 50% of the RBCs were restored to their original biconcave shape. Only those RBCs that showed no shape distortion were carefully selected for our measurements.

In each case, about 400 μl of the sample was taken in a holder which was made with a 1-mm-thick O-ring of diameter 0.8 cm stuck between two glass cover-slips. The arrangement was thus rendered air-tight.

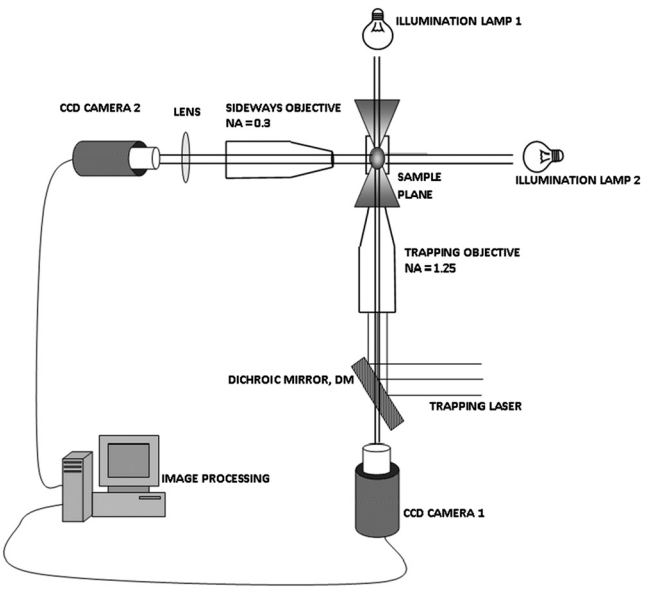

Fig. 1 Schematic of the setup to view along a direction perpendicular to the beam propagation direction.

2.2 *Other Details*

The optical tweezer setup used has been described in detail elsewhere.[7] Briefly, it consists of an Ytterbium fiber laser (1064 nm) guided into a 100 × (1.4 NA) oil immersion objective on a customized inverted microscope. The instrument is equipped with an XYZ stage and a provision for video imaging by a high speed CCD camera (200 frames/s, Voltrium, Singapore). For all the experiments discussed, the video imaging has been carried out at the rate of 10 frames/s, which translates to a time span of 70 ms for each frame. All measurements were carried out at room temperature (295 K).

To resolve the issue of RBC reorientation (flipping) versus folding[8] on being trapped in an optical tweezer, we have set up an imaging system capable of recording the view along a direction perpendicular to the beam propagation direction. A schematic of the setup is shown in Fig. 1.

All measurements of t_{re} were carried out by trapping RBCs at a height of 10 μm from the lower cover slip. To rule out influence of the cover slip on orientation time measurements, we have repeated measurements at trapping distances of 15 and 20 μm from the cover slip. We find identical features in the variation of t_{re} with P at all three trap distances and conclude that the trapping distance of 10 μm is free from any hydrodynamic influence of the cover slip.

The power measured beyond the objective and a cover slip was rescaled in accordance with Beer's law for absorptive loss for a 10-μm-thick layer of water to obtain the power P at the trap center. We have restricted laser powers to within 0.05 W ensuring that all our measurements are carried out in conditions where heating and convection effects due to the trap are minimal according to the criteria in Ref. 9. The power at the trap center was usually varied from about 0.002 W to a maximum of about 0.040 W. Beyond 0.024 W, it was important to subject the suspension to only short exposures of the laser beam to avoid any form of cell mutilation. Beyond 0.040 W, the mutilation process was observed to be instant.

3 Results and Discussion

3.1 *Flipping or Folding*

The process of RBC reorientation in an optical trap as viewed along the beam propagation direction (Z) can be seen in the series of photographs shown in Fig. 2 while a typical recording of the same can be seen in Video 1. Figure 3(a) shows a

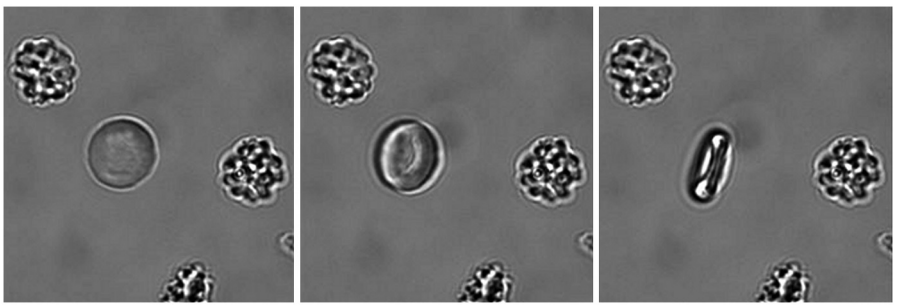

Fig. 2 A sequence of images showing the process of orientation of a human red blood cell in an optical trap as viewed along the beam propagation direction (Z). The images are separated temporally by 100 ms. (Video 1, MPEG, 5.28 MB) [URL: http://dx.doi.org/10.1117/1.JBO.18.2.025001.1].

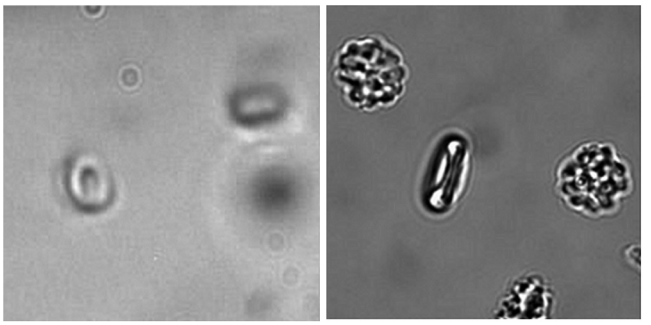

Fig. 3 (a) Trapped RBC viewed along a direction perpendicular to the beam propagation direction (*X*). (b) Trapped RBC viewed along the beam propagation direction (*Z*). (Video 2, MPEG, 2.26 MB) [URL: http://dx.doi.org/10.1117/1.JBO.18.2.025001.2].

photograph of the trapped RBC viewed along a direction perpendicular to the beam propagation direction (X) and shown alongside is the view of the same along Z [Fig. 3(b)]. Behavior of the trapped RBC on blocking and unblocking the trapping laser beam as viewed along X can be seen in Video 2. It is evident from these that no process other than a reorientation of the RBC occurs. In particular, there is no evidence of RBC folding as reported in Ref. 8. Rather, our observations are in accordance with those reported in Ref. 10.

3.2 *Theoretical Model of RBC Reorientation in an Optical Trap*

We present a mechanical model for RBC orientation in an optical trap treating the RBC as a perfectly rigid circular disc. We assume that at initial time $t = 0$, the plane of the RBC (represented by the solid black line in Fig. 4) is perpendicular to the direction of propagation of the laser beam (Z). The angle between the plane of the RBC at any given time and plane

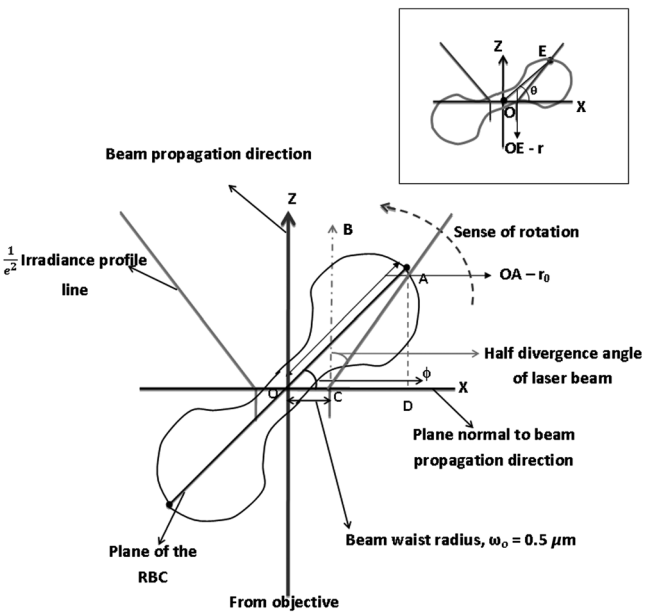

Fig. 4 Two-dimensional projection of the RBC reorientation process in an optical tweezer. The inset shows the reorientation process at an angle $\theta < \phi$, the angle of complete exposure of RBC surface to laser beam.

of the RBC at $t = 0$ is represented by θ, the angular displacement (see inset Fig. 4).

We make a further assumption that the geometric centre of the RBC is always coincident with the center of the laser beam waist in the optical trap. This means that at time $t = 0$, a circular area on the RBC whose radius r is equal to the laser beam waist is exposed to the laser light. As the RBC starts to reorient at time $t > 0$, the value of r changes. Thus r can be defined as the radius of the RBC surface exposed to the laser beam. After a certain angle, the entire RBC surface is exposed to the laser beam at which point r becomes equal to the value of the RBC radius (r_o). A calculation based on the beam geometry, taking r_o to be 4 μm, yields the value of this angle, ϕ to be 45.6 deg (Appendix 1). Thus for $\theta < \phi$, the value of r is a function of θ and can be calculated as detailed in appendix 2, while for $\theta > \phi$, r is just the RBC radius, r_o. Knowing the value of r for all θ, 0 deg $\leq \theta \leq$ 90 deg, we calculate the laser-generated torque acting on the RBC in the optical trap at all angles during the reorientation process.

The reorientation process of the RBC in an optical trap can be described by the rotational Langevin equation given below:

$$I\ddot{\theta} + \frac{32}{3}\eta r_0^3\dot{\theta} = \tau_{\text{laser}} + \tau_{\text{thermal}}, \tag{1}$$

where I is the moment of inertia of the RBC about the axis of flip, $\dot{\theta}$ and $\ddot{\theta}$ the first and second derivative of the angular displacement θ with respect to time, respectively, η the viscosity of the surrounding medium (here assumed to be same as that of water), r_o the radius of RBC and τ_{laser} and τ_{thermal}, the laser and thermal generated torques acting on the RBC, respectively. The factor (32/3) premultiplying the rotational drag term is the Perrin friction factor for a circular disk.[11]

Thermal torques are due to molecular collisions, which are random and active over time intervals much smaller than the measurement time frame and thereby average out. Thus the only torque that is relevant is the laser generated torque. We also find that the inertial term is three orders of magnitude smaller than the rotational drag term and five orders of magnitude smaller than the drive term for the process of RBC reorientation and thereby neglect it. Expanding τ_{laser} as $rF\sin(90 \text{ deg} - \theta)$, where $F = nP/c$, n being the index contrast between the RBC membrane and the surrounding liquid, P the incident laser power, and c is the velocity of light in vacuum, we get

$$\frac{32}{3}\eta r_0^3\dot{\theta} = r\frac{nP}{c}\cos\theta. \tag{2}$$

The Langevin equation is now solved independently for the two regions of θ; the first where $\theta < \phi$, and r is itself a function of θ and the second region, where $\theta > \phi$ and r takes the constant value of the RBC radius r_0. Integrating the relevant differential equations, we solve for the time required for the RBC to orient itself from $\theta = 0$ deg to ϕ and from $\theta = \phi$ to 90 deg, the sum of these two times being t_{re}. We have a final expression for t_{re}, given by

$$t_{re} = \frac{32}{3}\eta r_0^2 \times \frac{c}{nP} \times \left[\int_{0 \text{ deg}}^{\phi} \frac{r_0}{r\cos\theta}\,d\theta + \int_{\phi}^{90 \text{ deg}} \frac{d\theta}{\cos\theta}\right]. \tag{3}$$

Figure 5 shows us the theoretically predicted variation of t_{re} with P treating the RBC as a perfectly rigid circular disk.

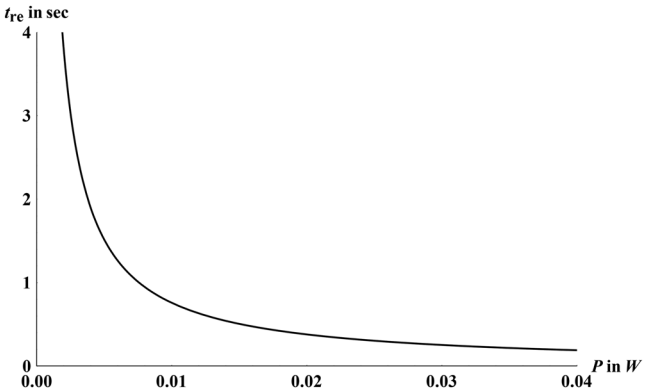

Fig. 5 Variation of t_{re} with P for a rigid circular disk of radius 4 μm.

A perfectly rigid circular disk is, however, only an approximation for a real RBC. We cannot expect the theoretically predicted variation of t_{re} with P to fit our experimental results unless we change the Perrin friction factor used to one that is more appropriate for an RBC. The experimentally determined t_{re} variation with P at very low powers can be expected to be closest to perfect rigid body behavior. We thereby use this variation at low powers to determine the appropriate drag term coefficient that can be used instead of the factor of (32/3) meant for a rigid circular disk in Eq. (3) to predict the variation for a real RBC.

3.3 *Normal RBC*

The recording of the RBC reorientation process was subjected to an image analysis routine to determine the number of frames required for an RBC whose plane is initially perpendicular to the beam propagation direction to undergo a 90-deg change in orientation which marks the end of the reorientation process. Knowing the time gap between two successive frames, the reorientation time (t_{re}) was calculated. At each power setting, at least 10 different RBCs were randomly picked from the sample under experimentation and t_{re} for each of them was determined. Average t_{re} as well the standard deviation in t_{re} at a particular power has been shown as a function of P for one of the RBC suspensions (*normal* RBC1) in Fig. 6(a). The standard deviation in the measurement of P for all the measurements carried out at a single laser power have been indicated as error bars in the x direction in this figure. Figure 6(b) shows the result of an identical set of measurements carried out in a different batch of RBC suspension with pH 7.4 (*normal* RBC2). It can be seen that though the broad features of the variation of t_{re} with P remain the same, the minor details are different. This is indeed the case with each of the different batches of RBC suspensions.

As the various PBS solutions prepared vary marginally in terms of their osmolarity, it is reasonable to conclude that the reorientation process of RBCs in an optical trap is sensitive to its chemical environment. Note that the rotational drag term in the Langevin equation used in the earlier section has a cubic dependence on the radius of the RBC and additionally a Perrin friction factor, which depends on the actual shape of the cell. If the surrounding suspension influences these factors, it is plausible that the effect on the rotational drag and thereby t_{re} is substantial. It is known that penetrating solutes can diffuse through a cell membrane dragging water molecules with them, thus causing changes in cell shape/volume. Similarly, nonpenetrating solutes cause osmosis of water from within the cell again leading to

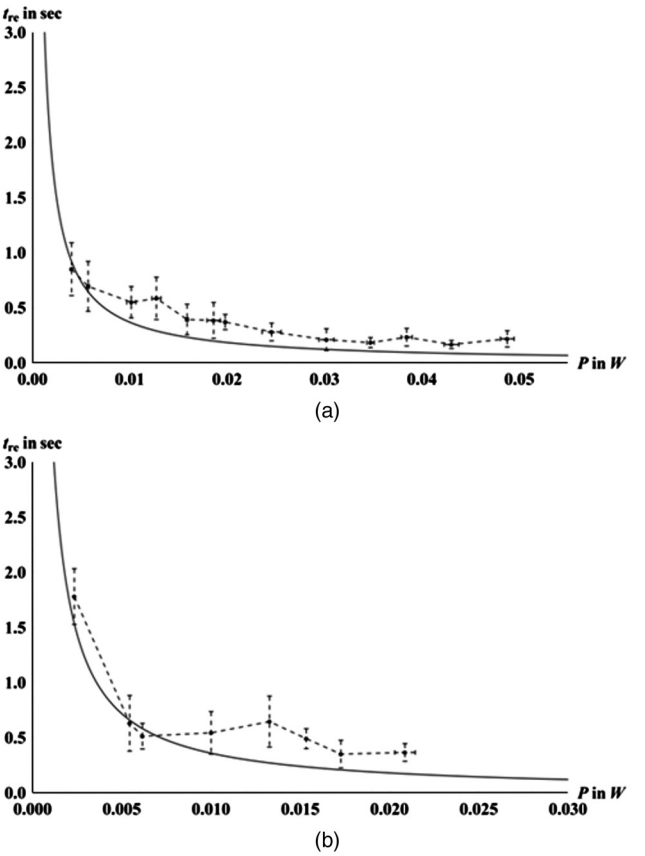

Fig. 6 (a) Variation of t_{re} with P for *normal* RBC1. The solid curve represents the rescaled rigid body behavior. The dashed curve is a guide to the eye. (b) Variation of t_{re} with P for *normal* RBC2. The solid curve represents the rescaled rigid body behavior. The dashed curve is a guide to the eye.

changes in cell shape/volume. Marginal changes in osmolarity of the PBS solution can thus cause changes to cell shape/volume which though not visually identifiable under a microscope have a telling effect on the features of t_{re} variation with P as a result of change in the drag torque. It is thereby necessary that appropriate Perrin friction factors are determined separately for every PBS solution where osmolarity may have varied.

Using the low power behavior as the closest approximation to a perfectly rigid body, we determine the Perrin friction factor and using this instead of the factor of (32/3) appropriate for a rigid disc in Eq. (3), predict the variation of t_{re} with P for a perfectly rigid body having a rotational drag identical to the RBC under study. In carrying out the fit the greatest weight is assigned to the value measured at the lowest power. The fits thus generated have been shown in Fig. 6(a) and 6(b) using solid lines. As can be seen from the figures, the measured variation of t_{re} with P deviates from the predicted rigid body behavior beyond a value of power P_d.

In principle, such a deviation is possible if there is a change in the rotational drag coefficient. However, if this coefficient were to remain constant above P_d then the variation of t_{re} with P would still show an inverse power dependence for $P > P_d$ albeit with an alteration. Comparing all the RBCs studied, we find that a straight line describes the closest possible fit for the values of t_{re} at $P > P_d$ which indicates a rotational drag that varies continuously with the impingent power. This indicates deformation.

Measurement of t_{re} for $P > 25$ mW without damage to the trapped RBCs was possible only for one *normal* RBC sample set. The variation of t_{re} with P for $P > 25$ mW could not be described by the linear fit that was found to be valid for $P_d < P < 25$ mW. Rather, it was an inverse power dependence, as expected for a rigid body, that best described the variation. The reorientational dynamics of an RBC in an optical tweezer can thereby be possibly summed up as (1) rigid-body-like behavior at low laser powers; (2) an intermediate range of powers where the body is deformed, and there is marked deviation from rigid-body-like behavior, and (3) a return to rigid-body-like behavior at still higher powers when additional deformations are energetically unfeasible. While this appears plausible, it is possible to arrive at erroneous conclusions for $P > 25$ mW. The values of t_{re} are low here and being limited by the frame rate of our camera, we cannot measure t_{re} with enough precision to make a conclusion about its variation with P. We thereby limit the rest of our discussion to the behavior of the RBCs in the $P < 25$ mW range and what we can extrapolate from it.

While there is evidence that the RBCs are deformed from their original shape/volume during the process of reorientation in an optical trap, this experimental technique is limited in its ability to qualify the deformation. Neither can a chronology to the events of deformation and rotational flip during the process of reorientation be assigned. Nonetheless it is reasonable to assume that the cell content, being akin to water, is similar to an incompressible fluid and does not undergo any appreciable change in volume during the reorientation process given the kind of forces and torques possible at the laser power range used. The deformation, thereby, is predominantly from changes in shape/volume of the RBC that involve processes of RBC membrane compression or shear. The RBC membrane referred to here is a composite of the phospholipid bilayer, the underlying spectrin-based cytoskeleton as well as all the transmembrane proteins in accordance to the description of the RBC membrane given in Refs. 12 and 13. Note that this composite view of the RBC membrane is in contrast with the view held by other scientists in the field,[14] where the cytoskeleton is not considered to be a part of the RBC membrane. However, as our experimental technique is incapable of distinguishing between the viscoelastic contributions of the various components of the membrane, adhering to the composite view of the membrane does not detract from our argument.

4 Estimation of Excess Energy Used During RBC Reorientation in an Optical Trap

As can be seen from Fig. 6(a) and 6(b), the experimentally determined t_{re} are greater than the theoretically predicted t_{re} at all powers greater than P_d at which the experiment could be carried out. We fit a straight line through the experimental values of t_{re} for P such that $P_d \le P \le 25$ mW. The straight line fit is extrapolated to values of P beyond 25 mW where measurements may not actually have been carried out. We compute the quantity

$$\Delta E = \frac{\pi}{2}\left[\tau_{\text{laser}} - \alpha\frac{32}{3}\eta r_0^3\dot{\theta}_{\text{experiment}}\right] - \frac{\pi}{2}\left[\tau_{\text{laser}} - \alpha\frac{32}{3}\eta r_0^3\dot{\theta}_{\text{therory}}\right], \quad (4)$$

where $\alpha(32/3)$ is the appropriate Perrin friction factor for the RBC and $\dot{\theta}_{\text{experiment}}$ and $\dot{\theta}_{\text{theory}}$ are the average angular speeds estimated from the straight line fit to the experimental values and that predicted by the theory outlined in Sec. (2), respectively. This quantity represents an amount of energy that is utilized for the reorientation process of the RBC in excess of that which is predicted for a rigid body with identical rotational drag coefficient. Thus we have

$$\Delta E = \frac{\pi}{2}\alpha\frac{32}{3}\eta r_0^3\left[\frac{\pi/2}{t_{\text{re(theory)}}} - \frac{\pi/2}{t_{\text{re(experiment)}}}\right]. \quad (5)$$

Figure 7 shows the variation of ΔE with P for *normal* RBC1 and *normal* RBC2. Note again that we have plotted ΔE even at values of P where measurement could not be carried out because of cell mutilation on exposure to the laser beam by extrapolating from the behavior of the RBC at P such that $P_d \le P \le 25$ mW where measurements were actually done. The actual experimental values as well as the standard deviation on them have also been shown on the plot.

ΔE being the excess energy utilized in the reorientation process due to departure in behavior of the RBC from that of a perfect rigid body, can be considered to be an indicator of the viscoelastic response of the same. ΔE could be partitioned into (1) work done in deforming the body, which would be a signature of the elastic behavior of the RBC membrane and (2) dissipation because of viscous effects arising from the membrane (membrane viscosity) and/or the cell contents (cytoplasmic viscosity). The manner of this partition would depend on the precise mechanical model invoked to represent the RBC membrane.

The stress the RBC is subjected to in a reorientation process in the tweezer is small. No visible deformations can be identified under the microscope during any point of the process. Contrast this with the case of fluid shear stress application, micropipette aspiration or optical stretcher techniques,[13–22] where the RBC is subjected to stresses capable of causing large visible deformations. Given that the stress involved is low, the response of the system can be assumed to be within the linear viscoelastic range. Based on this, one could further assume that the ratio of the work done in deforming the RBC to the dissipation because of viscous effects remains the same at all the powers. Further, as we are unable to measure a finite time over which the RBC relaxes following the reorientation, we conclude that the viscous effects in this stress range are minimal. Thus the maximum value of ΔE (ΔE_{max}) represents the situation of maximum energy that has gone into deformation. If we assume that the elastic property of the RBC membrane remains a constant at all powers, this will represent the situation of maximum deformation allowed in the process of reorientation. We tabulate ΔE_{max} and the power at which ΔE_{max} is recorded for *normal* RBC1 and *normal* RBC2 in Table 1. As can be seen, the values for the two separate data sets corroborate well with each other.

If we conjecture that the departure of the dynamical behavior of an RBC from that of a rigid body with an identical rotational drag coefficient is strongly influenced by the nature of the RBC membrane, the quantity ΔE_{max} must have a strong dependence on the elasticity of the RBC membrane. This is because it should cost more energy to deform a stiffer membrane than a more pliable one to the same extent. The study of two contrasting cases outlined below lends credence to this conjecture.

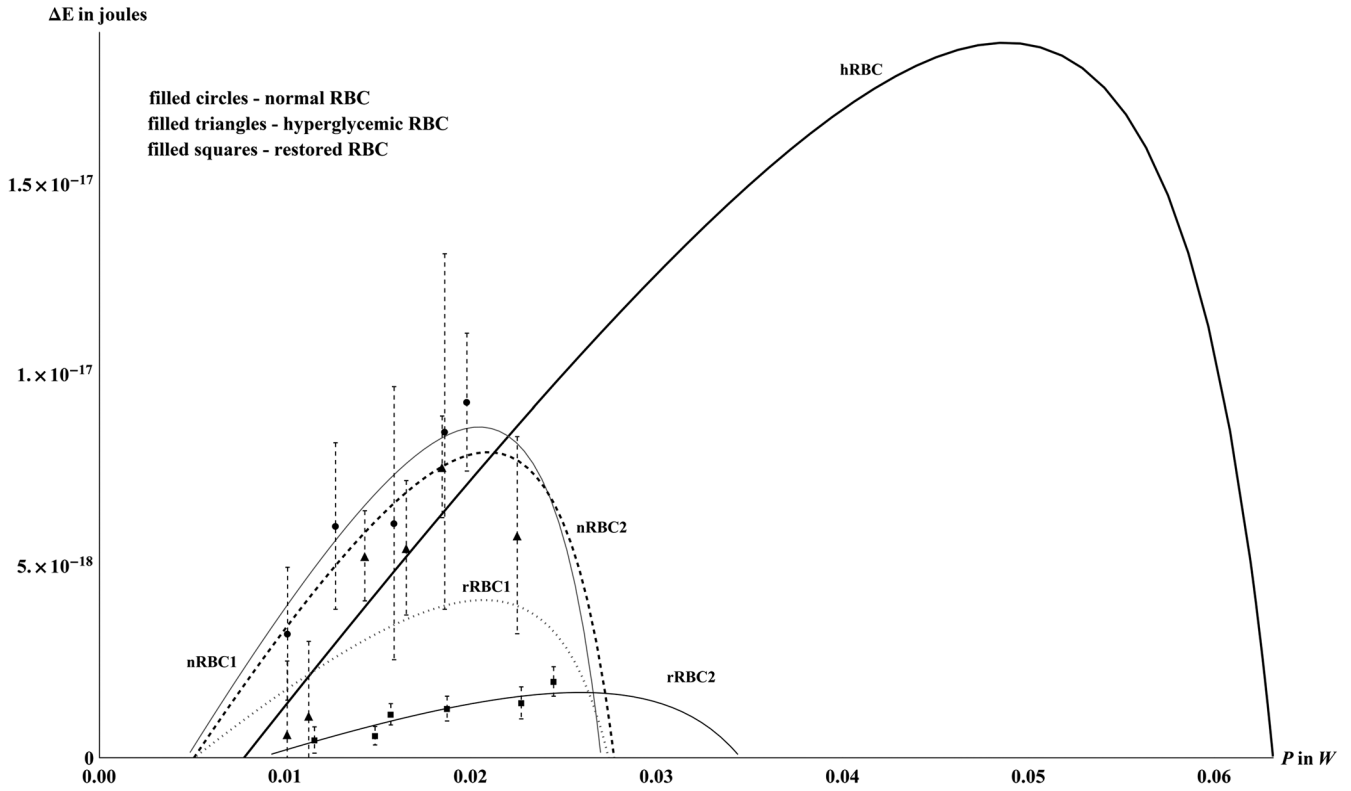

Fig. 7 Variation of ΔE with P for *normal* RBC1 (thin gray curve, filled circles), *normal* RBC2 (thick black dashed curve), *h*RBC (thick black curve, filled triangles), *r*RBC1 (gray dotted curve), and *r*RBC2 (thin black curve, filled squares).

Table 1 Tabulation of ΔE_{max} for all types of RBCs.

Data set	$P(W)$ for E_{max}	$\Delta E_{max} \times 10^{-18}$ joule	Spread in $\Delta E_{max} \times 10^{-18}$ joule
Normal RBC1	0.0205	8.6	1.95
Normal RBC2	0.0209	8.0	1.85
*h*RBC	0.0327	18.7	2.16
*r*RBC1	0.0216	4.1	0.31
*r*RBC2	0.0258	1.7	0.57

4.1 *h*RBC

Figure 8 shows the variation of t_{re} with P for *h*RBC. The variation of t_{re} with P for *normal* RBC suspended in the same PBS solution that was used for the *h*RBC measurements has also been shown in Fig. 8 as a comparison of the two cases can be carried out here. The rigid body fits generated by the method outlined earlier are shown as solid lines. We find that P_d for *h*RBC is greater than that of *normal* RBC. Figure 7 shows the variation of ΔE with P for *h*RBC while the value of ΔE_{max} for *h*RBC has been tabulated in Table 1. It can be seen that the value of ΔE_{max} for *h*RBC is greater than that for *normal* RBC.

4.2 *r*RBC

It has been reported in literature that initial stages of crenation are completely reversible.[23] We have worked here with two batches of RBCs, which were subjected to processes of crenation and restoration. The process for the two batches may be different in details beyond the experimental control possible in our laboratory, and so we report the findings separately (data sets *r*RBC1 and *r*RBC2). The dynamics of the reorientation process in *r*RBCs were observed to be much more complex than those of *normal* RBCs,[24] in general. The values of t_{re} were consistently higher than those measured for *normal* RBC at the same P. This was irrespective of which batch of PBS was used as the medium of suspension. Figure 9 shows the variation of t_{re} with P for *r*RBC along with that for *normal* RBC clearly demonstrating this. We conclude that even initial stages of crenation are not completely reversible in terms of all properties of the RBC. So while *r*RBCs appear like *normal* RBCs under a microscope, their behavior in an optical trap is altered. Rigid body fits generated by the method outlined earlier are shown in Fig. 9 as solid lines. The variation of ΔE with P for rRBC has been shown in Fig. 7. The values of ΔE_{max} for both data sets, *r*RBC1 and *r*RBC2, have been tabulated in Table 1. We note that both these values are substantially smaller than the value for *normal* RBC.

Cytoplasmic viscosity in RBC is determined by intracellular hemoglobin concentration.[12] The *h*RBCs used in our experiment are sourced from a volunteer with an established case of hyperglycemia but with intracellular hemoglobin content within the range expected of a healthy individual. *r*RBCs are restored from *normal* RBCs subjected to crenation. This being the case we can expect that the cytoplasmic viscosity is the same in the case of the *normal* RBC, *h*RBC, and *r*RBC. The vast differences in the values of ΔE_{max} for the three cases cannot thereby be attributed to cytoplasmic viscosity. This must be arising then from the difference in the RBC membrane viscoelastic response

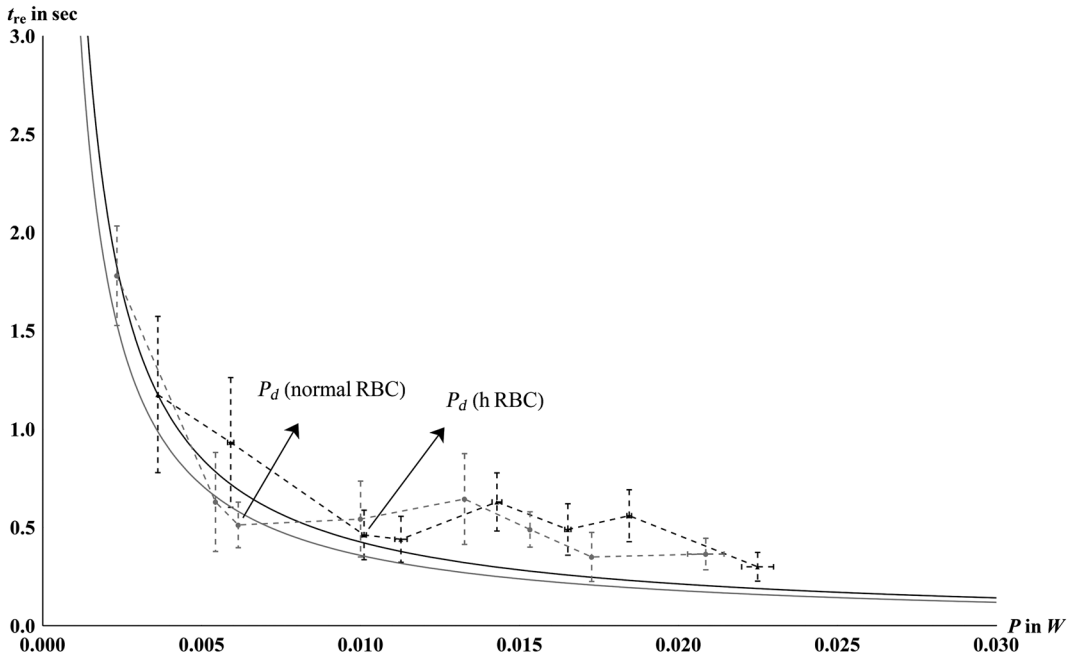

Fig. 8 Variation of t_{re} with P for (a) *h*RBC (black) and (b) *normal* RBC2 (gray). The dashed curves are guides to the eye. The gray solid curve is rescaled rigid body curve for normal RBC and the black solid curve is rescaled rigid body curve for *h*RBC. Note that P_d for *h*RBC (0.01 W) is greater than that for *normal* RBC (0.006 W)

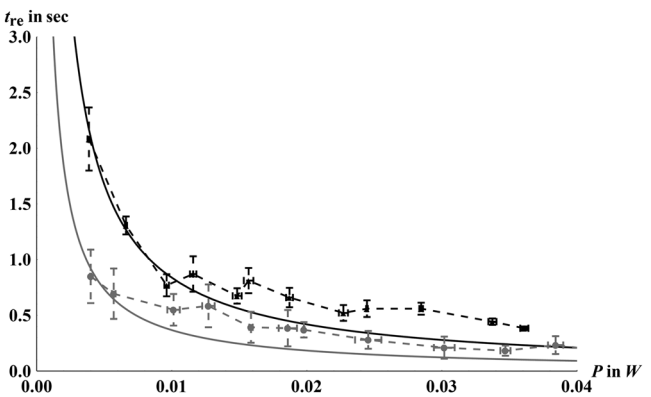

Fig. 9 Variation of t_{re} with P for (a) *r*RBC (black) and (b) *normal* RBC1 (gray). The dashed curves are a guide to the eye; the black dashed curve represents the experimental data for *r*RBC, and the gray dashed curve represents the data for *normal* RBC1. The black solid curve represents the rescaled rigid body theory for *r*RBC, and the gray solid curve represents the rescaled rigid body curve for *normal* RBC1. Note that the values of t_{re} are consistently higher for *r*RBC than that for *normal* RBC at the same P.

for the three types of RBC. We have concluded earlier that at the stress range the RBC is subjected to in the optical tweezer, the RBC membrane elasticity dependent contribution to ΔE is dominant. ΔE_{max}, then, is an indicator of the stiffness of a membrane. Our earlier findings of higher angular speeds after reorientation in *h*RBC, which we attributed to stiffening of the membrane of RBCs exposed to hyperglycemic conditions[6] are consistent with the current study which points towards an increase in membrane stiffness for these cells. In the case of the *r*RBCs, the findings are consistent with a lowering in membrane stiffness as compared to *normal* RBCs. The membrane elasticity, however, appears to be affected to different extents for the two batches.

One can expect that the absolute values of t_{re} at the same P will be lower for stiffer membranes. It is, however, essential to exercise caution while carrying out comparisons of relative values of t_{re} unless the medium of suspension used in the measurement is identical.

In all the measurements carried out, a clear signature of RBC deformation during reorientation in an optical trap is present post a power P_d. P_d, in itself, can be expected to serve as an indicator of membrane stiffness. However, it is possible that deformations to the RBC shape/volume happen at the lowest trapping powers. We are unable to identify this process because we use the data at the lowest powers to compute the drag coefficient and predict the rigid body variation of t_{re} with P. P_d can be said to be the power at which the RBC deformations are large enough to manifest in behavior clearly different from that at low power. This value, thereby, depends on the manner in which the rigid body behavior is computed. Comparisons of values of P_d can be done provided the method of predicting the rigid body behavior is identical in addition to the medium of suspension used in the measurement.

The last four decades have witnessed an intense interest in the mechanical properties of human red blood cells, and a wide variety of techniques have been employed over this time span to measure the various elastic moduli associated with it. The methods of application of fluid shear stress, micropipette aspiration or optical tweezer based stretching techniques[13–22] involve deforming the RBC (the degree of control over the deformation and the exact estimate of the deforming force varying for each of the techniques), and an estimate of the viscoelastic constants is made from the study of the extent of the deformation and the manner of relaxation to the original dimensions. The elastic moduli estimated from these studies have a rather wide range owing perhaps to the differences in the mechanical model assumed for the RBC in each case. Reference 25 reports a measurement of the dynamic storage and loss moduli of the RBC

membrane from studies of driven fluctuations brought about by an oscillatory magnetic field acting on a ferrimagnetic bead attached to the membrane (magnetic twisting cytometry). All these methods suffer from the inability to detract from the measurements the effect of the contact probes themselves. More recent efforts involve the estimation of the elastic moduli from optical interferometry/diffraction phase microscopy based studies of the nanoscale fluctuations of the RBC membrane.[26–29] The technique used by us is simple and uncomplicated in comparison and tests the viscoelastic response of the RBC at a stress range lower than that found in the techniques of fluid shear stress application, micropipette aspiration, or optical tweezer based stretching. While it cannot estimate the elastic moduli independent of other methods, it gives a gauge of the complete viscoelastic response of the RBC. This may be a factor of great relevance for gauging the efficiency of circulation of the RBC in the human vasculature. It can also be extremely useful for purposes of comparison between healthy and diseased cells. While an independent estimate of the elastic moduli using the technique outlined in this work is not possible, an estimate of the elastic moduli of the different RBC types (here *h*RBC and *r*RBC) can be made based on the value for the *normal* RBC determined by a different technique. Assuming that the viscous effects in this stress range are minimal, a rough estimate of the maximum deformation possible in the reorientation process in an optical tweezer for *normal* RBC can be made using a value of 2.5×10^{-6} N/m for RBC shear modulus reported in Ref. 21 and the value of $\Delta E_{\max}$ estimated by our method. Making a crude assumption that the deformation remains the same for *h*RBC as well as *r*RBC, we can set a lower limit of 5.8×10^{-6} N/m for the shear modulus of *h*RBC and an upper limit of 0.53×10^{-6} N/m for the shear modulus of *r*RBC.

5 Conclusion

We report here on the variation of time of reorientation of RBCs in an optical trap with laser power. We compare the experimentally determined variation with that expected for a rigid body having a rotational drag determined from the low power behavior where maximum adherence to rigid-body-like behavior can be assumed. We further determine the energy cost arising from the viscoelastic response of the RBC. We find that the maximum energy cost possible during reorientation, scales as the stiffness of the RBC membrane. We conclude thereby that this fairly simple measurement can yield information about the elasticity of the RBC membrane.

The elasticity of the RBC membrane is a very important property for the RBC as they often flow through capillaries with diameters much smaller than their own: It is extremely important that RBCs are able to move through these narrow channels in the circulatory system without compromising their function during their lifespan of about 100 to 120 days. An altered elasticity of the RBC membrane may be a first recognizable pointer for a serious underlying medical condition. We have shown here that RBCs exposed to hyperglycemic conditions have stiffer membranes than those sourced from healthy individuals with no chronic medical conditions. It is maybe worthwhile thereby to develop a simple nondestructive experimental technique that could gauge RBC membrane stiffness for use as a diagnostic tool. The method outlined in this study could form the basis for such a technique.

Appendix 1: Computation of Angle of Complete Exposure of RBC Surface to the Laser Beam (φ)

The half divergence angle for a Gaussian laser beam is given by $\gamma = (\lambda/\pi\omega_o)$ (Ref. 30) where, λ is the wavelength of the laser, and ω_o is the beam waist radius of the laser. Taking $\lambda = 1064$ nm and $\omega_o = 0.5$ μm, this angle is found to be 38.8 deg. With reference to Fig. 4, angle AOC is θ, the instantaneous angle made by the RBC plane with the plane normal to the beam propagation direction. At the position of complete exposure of RBC surface to the laser light, at $\theta = \phi$. The length AO, which represents the RBC radius, can be taken to be 4 μm. From geometric considerations it can be seen that

$$\phi = \tan^{-1}\left[\frac{x\,\tan(\frac{\pi}{2}-\gamma)}{\omega_0 + x}\right], \tag{6}$$

where x is the length CD which can be solved for using the Pythagoras theorem for triangle AOD. Our calculations yield $\phi = 45.6$ deg.

Appendix 2: Determination of r for $\theta < \phi$

From geometric considerations it can be seen that r is given by

$$r = \sqrt{\left\{(x+\omega_0)^2 + \left[x\,\tan\left(\frac{\pi}{2}-\gamma\right)\right]^2\right\}}, \tag{7}$$

where x can be solved for from the relation

$$(x+\omega_0)\tan\theta = x\,\tan\left(\frac{\pi}{2}-\gamma\right). \tag{8}$$

Acknowledgments

The authors would like to acknowledge a project grant from the Department of Science and Technology (DST), government of India (Nano mission programme). The authors also acknowledge Dr. Manas Khan and Prof. A. K. Sood for the kind provision of chemicals and Mr. B. R. Parthasarathi for valuable assistance. One of the authors (P. Praveen) acknowledges Mr. Sujith Thomas for useful discussions.

References

1. R. C. Gauthier, "Theoretical investigation of the optical trapping force and torque on cylindrical micro-objects," *J. Opt. Soc. Am. B* **14**(12), 3323–3333 (1997).
2. R. C. Gauthier, M. Ashman, and C. P. Grover, "Experimental confirmation of the optical-trapping properties of cylindrical objects," *Appl. Opt.* **38**(22), 4861–4869 (1999).
3. Z. Cheng, P. M. Chaikin, and T. G. Mason, "Light streak tracking of optically trapped thin microdisks," *Phys. Rev. Lett.* **89**(10), 108303 (2002).
4. E. Higurashi, R. Sawada, and T. Ito, "Optically induced angular alignment of trapped birefringent micro-objects by linearly polarized light," *Phys. Rev. E* **59**(3), 3676–3681 (1999).
5. M. Khan, S. K. Mohanty, and A. K. Sood, "Optically driven red blood cell rotor in linearly polarized laser tweezers," *Pramana* **65**(5), 777–786 (2005).
6. B. V. Nagesh et al., "Rotational dynamics of RBC in an optical trap as a medical diagnostic technique," in *Proc. NANO 2010*, Tiruchengode, Tamilnadu, India, p. 141, Macmillan Publishers India Ltd., New Delhi (2010).

7. Yogesha et al., "A dual optical tweezer for microrheology of bacterial suspensions," *Int. J. Nanosci.* **10**(1–2), 181–186 (2011).
8. A. Ghosh et al., "Euler buckling-induced folding and rotation of red blood cells in an optical trap," *Phys. Biol.* **3**(1), 67–73 (2006).
9. E. J. G. Peterman, F. Gittes, and C. F. Schmidt, "Laser-induced heating in optical traps," *Biophys. J.* **84**(2), 1308–1316 (2003).
10. K. Mohanty et al., "Orientation of erythrocytes in optical trap revealed by confocal fluorescence microscopy," *JBO Lett.* **12**(6), 060506 (2007).
11. H.C. Berg, *Random Walks in Biology*, p. 84, Princeton University Press, Princeton, New Jersey (1993).
12. N. Mohandas and P. G. Gallagher, "Red cell membrane: past, present and future," *Blood* **112**(10), 3939–3948 (2008).
13. G. Lenormand et al., "Direct measurement of the area expansion and shear moduli of the human red blood cell membrane skeleton," *Biophys. J.* **81**(1), 43–56 (2001).
14. Y-Z. Yoon et al., "The non-linear mechanical response of the red blood cell," *Phys. Biol.* **5**(3), 036007 (2008).
15. R. M. Hochmuth, N. Mohandas, and P.L. Blackshear Jr., "Measurement of the elastic modulus for the red cell membrane using a fluid mechanical technique," *Biophys. J.* **13**(8), 747–762 (1973).
16. E. A. Evans and R. Skalak, *Mechanics and Thermal Dynamics of Biomembranes*, CRC Press, Boca Raton, Florida (1980).
17. R. M. Hochmuth, "Properties of red blood cells," in *Handbook of Bioengineering*, R. Skalak and S. Chien, Eds., McGraw Hill, Inc., New York (1987).
18. Y. C. Fung, *Biomechanics: Mechanical Properties of Living Tissues*, Springer-Verlag, New York (1993).
19. D. E. Discher, D. H. Boal, and S. K. Boey, "Simulations of the erythrocyte cytoskeleton at large deformation. II. Micropipette aspiration," *Biophys. J.* **75**(3), 1584–1597 (1998).
20. J. Sleep et al., "Elasticity of the red cell membrane and its relation to hemolytic disorders: an optical tweezer study," *Biophys. J.* **77**(6), 3085–3095 (1999).
21. S. Henon et al., "A new determination of the shear modulus of the human erythrocyte membrane using optical tweezers," *Biophys. J.* **76**(2), 1145–1151 (1999).
22. D. Boal, *Mechanics of the Cell*, Cambridge University Press, Cambridge (2002).
23. M. W. Gedde, E. Yang, and W. H. Huestis, "Shape response of human erythrocytes to altered cell pH," *Blood* **86**(4), 1595–1599 (1995).
24. B. V. Nagesh et al., "Normal human red blood cell shows birefringence," *manuscript under preparation*.
25. M. Puig-De-Morales-Marinkovic et al., "Viscoelasticity of the human red blood cell," *Am. J. Physiol. Cell Physiol.* **293**(2), C597–C605 (2007).
26. G. Popescu et al., "Optical measurement of cell membrane tension," *Phys. Rev. Lett.* **97**(21), 218101 (2006).
27. J. Evans et al., "Fluctuations of the red blood cell membrane: relation to mechanical properties and lack of ATP dependence," *Biophys. J.* **94**(10), 4134–4144 (2008).
28. Y. K. Park et al., "Measurement of red blood cell mechanics during morphological changes," *Proc. Natl. Acad. Sci. U. S. A.* **107**(15), 6731–6736 (2010).
29. Y. K. Park et al., "Measurement of nonlinear elasticity of red blood cell membranes," *Phys. Rev. E* **83**(5), 051925 (2011).
30. F. L. Pedrotti, L. S. Pedrotti, and L. M. Pedrotti, *Introduction to Optics*, 3rd ed., p. 589, Pearson Prentice Hall, Upper Saddle River, New Jersey (2007).